



# Chemical kinetics and interactions involved in horseradish peroxidase-mediated oxidative polymerization of phenolic compounds

Wenjing Cheng, Willie F. Harper Jr.\*

Department of Civil and Environmental Engineering, University of Pittsburgh, Pittsburgh, PA 15261, United States

## ARTICLE INFO

### Article history:

Received 12 October 2011

Received in revised form 1 December 2011

Accepted 22 December 2011

### Keywords:

Oxidative coupling

Estrogens

Wastewater

Horseradish peroxidase (HRP)

Solvent interactions

Thermodynamics

## ABSTRACT

The primary objective of this research was to evaluate various factors that affect the reaction rate of oxidative coupling (OXC) reaction of phenolic estrogens catalyzed by horseradish peroxidase (HRP). Kinetic parameters were obtained for the conversion of phenol as well as natural and synthetic estrogens estrone ( $E_1$ ), 17 $\beta$ -estradiol ( $E_2$ ), estriol ( $E_3$ ), and 17 $\alpha$ -ethinylestradiol ( $EE_2$ ). Molecular orbital theory and Autodock software were employed to analyze chemical properties and substrate binding characteristics. Reactions were first order with respect to phenolic concentration and reaction rate constants ( $k_r$ ) were determined for phenol,  $E_3$ ,  $E_1$ ,  $E_2$  and  $EE_2$  (in increasing order). Oxidative coupling was controlled by enzyme–substrate interactions, not collision frequency. Docking simulations show that higher binding energy and a shorter binding distance both promote more favorable kinetics. This research is the first to show that the OXC of phenolics is an entropy-driven and enthalpy-retarded process.

Published by Elsevier Inc.

## 1. Introduction

Researchers have oxidatively polymerized phenolic chemicals with horseradish peroxidase (HRP) to remediate wastewater [1–4]. Oxidative coupling (OXC) is fast and produces insoluble polymers that can be removed in sedimentation or filtration steps. The HRP-OXC catalytic cycle involves: (1) a hydrogen peroxide-induced transfer of two electrons from the iron (III) residue present at the active site of HRP, (2) a one-electron reduction step in which a phenolic substrate donates an electron to the HRP iron (IV)<sup>+</sup> residue, (3) a second one-electron reduction step in which a phenolic substrate donates an electron to the HRP iron (IV) residue, and (4) reaction between the two phenoxy radicals, resulting in the formation of dimers. These reaction products may in turn go on to participate in further coupling cycles, yielding higher order oligomer products. HRP-OXC is not as energy intensive as other advanced oxidation processes (i.e. ozonation), and compared to microbial degradation, HRP-OXC is faster and does not present concerns about metabolite toxicity because the byproducts are not soluble. HRP-OXC now stands as a promising and potentially sustainable option for addressing the presence of phenolic chemicals (including some endocrine disruptors) in water.

Researchers have used molecular orbital theory in an attempt to construct quantitative structure-activity relationships (QSAR) that inform HRP-OXC; these results have produced intriguing but

at times inconsistent correlations. Several studies showed varying levels of success in generating correlations between the turnover number ( $k_{cat}$ ) and energy of the highest-occupied molecular orbital ( $E_{HOMO}$ ) (i.e. between 0.560 and 0.998 [1,5–8]). Correlations between  $k_{cat}$  and the energy of the lowest unoccupied molecular orbital ( $E_{LUMO}$ ) have also produced mixed results for substituted phenols [6–8]. More recent efforts have accounted for enzyme–substrate binding features. Colosi et al. 2006 [1] found that the HRP reactivity is related to the binding distance with respect to histidine-42 residue of the HRP/substrate binding complex. Colosi et al. 2010 [9] went on to engineer HRP proteins in which the active pocket was opened, and they found that HRP reactivity (i.e.  $k_{cat}$ ) was reasonably correlated ( $R^2 = 0.81$ ) with predicted binding distances. This previous work highlighted the importance of enzyme–substrate binding features. There are, however, other hitherto undetermined factors which influence enzyme–substrate interaction. These include critical thermodynamics parameters (e.g. enthalpy and entropy of activation) and enzyme–substrate binding energy. It is also important to consider the participation of water molecules in OXC reactions occurring in the aqueous phase [10].

The overall objective of the current work is to examine the kinetics and reaction mechanisms associated with HRP-OXC, and particular attention is directed to issues that inform enzyme–substrate interactions. The specific aims are to evaluate (1) reaction kinetics over a range of temperatures, (2) kinetic limitations, (3) enzyme–substrate interactions, and (4) thermodynamic parameters. Five phenolic substrates (phenol,  $E_1$ ,  $E_2$ ,  $E_3$ ,  $EE_2$ ) were polymerized during laboratory testing.

\* Corresponding author. Tel.: +1 412 624 9548; fax: +1 412 624 0135.

E-mail address: [wharper@pitt.edu](mailto:wharper@pitt.edu) (W.F. Harper Jr.).

## 2. Materials and methods

### 2.1. Experimental overview

The phenolic substrates were spiked into synthetic wastewater held in 150 ml beakers and mixed with magnetic stir bars. The reaction kinetics and orders were determined by obtaining the initial reaction rate over a range of phenolic concentrations (i.e. 1  $\mu\text{M}$ –26  $\mu\text{M}$ ). The enthalpy of activation ( $\Delta H^*$ ) and entropy of activation ( $\Delta S^*$ ) were determined with data collected at different temperatures (5 °C, 15 °C, 25 °C, 35 °C). The  $E_{\text{HOMO}}$  was determined with the Gaussian 03 program and the molecular volume for each substrate was determined by dividing their molecular weights by their respective densities. The enzyme–substrate interactions were simulated with AutoDock 4.2 to determine binding energies and binding distances.

### 2.2. Materials

The following materials were purchased from Sigma–Aldrich (St. Louis, MO): phenol (CAS 108–95–2), steroidal hormones E<sub>1</sub> (CAS 53–16–7), E<sub>2</sub> (CAS 50–28–2), E<sub>3</sub> (CAS 50–27–1), EE<sub>2</sub> (CAS 57–63–6), hydrogen peroxide (50 wt%, CAS 7722–84–1), extracellular horseradish peroxidase (type I, R<sub>z</sub> = 1.3), polyethylene glycol (CAS 25322–68–3), 4-aminoantipyrine (AAP) (CAS 83–07–8), reagent-grade acetonitrile (CAS 75–05–8), and methanol (CAS 67–56–1).

### 2.3. Enzyme activity assay

A colorimetric assay was used to measure the HRP activity and concentration. The enzyme activity is proportional to the production rate of a constituent that absorbs light at a peak wavelength of 510 nm and with an extinction coefficient ( $\epsilon$ ) of 7100 M<sup>-1</sup> cm<sup>-1</sup>. The assay mixture consisted of 10 mM phenol, 2.4 mM AAP, and 0.2 mM H<sub>2</sub>O<sub>2</sub>. One unit of activity (U) was defined as the number of micromoles of hydrogen peroxide utilized per minute at pH 7.4 and 25 °C [11]. Absorbance was monitored at 510 nm with a UV–vis spectrophotometer (Spectronic 20, Bausch & Lomb) every 5 s for 1 min following a reaction initiation. All assays were performed in triplicate. Relative standard deviations (RSD) of triplicate measurements were always less than 5%.

### 2.4. Initial reaction rate

The initial reaction rate was determined for each kinetic test [12]. The HRP–OXC reactions were carried out at 25 °C in 100 ml of phosphate buffer (50 mM, pH = 7.0) using 150 ml beakers with various initial concentrations of substrate and a fixed dosage of HRP and H<sub>2</sub>O<sub>2</sub>. PEG was added to protect HRP from oxidative damage, as suggested by [13]. Methanol stock solutions were made for E<sub>1</sub>, E<sub>2</sub>, E<sub>3</sub> and EE<sub>2</sub> at 1 mM, and the reaction mixtures were prepared by diluting the stock solution to the desired concentration (between 1  $\mu\text{M}$  and 26  $\mu\text{M}$ ). For phenol, the 1 mM stock solution was made in water. The batch reactors were mixed at 300 rpm with a Teflon-coated magnetic bar at neutral pH. Each reactor contained the appropriate mass of substrate, 10  $\mu\text{M}$  H<sub>2</sub>O<sub>2</sub>, and 30 mg/l PEG, and the reaction was initiated by adding HRP. The initial HRP activity was 0.37 U/ml. The 10  $\mu\text{M}$  H<sub>2</sub>O<sub>2</sub> concentration was selected to obtain a molar peroxide-to-substrate ratio of 2.0–5.0, as suggested by previous work [3,14,15]. During the tests, 2-ml aliquots were taken from the batch reactors every 10 s for the first 20 s, and the reaction was stopped by adding 0.1 ml of 10% phosphoric acid. The acidified samples were then filtered through a 0.45- $\mu\text{m}$  syringe filter (Pall Life Science Inc., Ann Arbor, MI). Each experiment was done in triplicate.

### 2.5. HPLC analysis of phenolic substrates

The phenolic substrate concentrations were measured with an Agilent 1200 series high-performance liquid chromatograph (HPLC) equipped with an Elipse XDB-C18 column (150 mm  $\times$  4.6 mm, 5  $\mu\text{m}$  particle size). The concentrations were determined with UV absorbance (wavelength = 197 nm) with external calibration. The mobile phase consisted of 40% reagent-grade acetonitrile (ACN) and 60% deionized water (DI). The flow rate was 1.0 ml/min. The retention times for each substrate were 3.03 min (phenol), 12.31 min (E<sub>1</sub>), 7.27 min (E<sub>2</sub>), 2.05 min (E<sub>3</sub>), and 10.24 min (EE<sub>2</sub>).

### 2.6. Kinetic and thermodynamic determination

The initial reaction rate ( $v_a$ ) is related to the substrate concentration as shown in the following equation [12]:

$$v_a = \left| \frac{d[A_0]}{dt} \right| = (k[B_0]^m)[A_0]^n = k_f[A_0]^n \quad (1)$$

where A represents the substrate, B is H<sub>2</sub>O<sub>2</sub>,  $k_f$  is a reaction rate constant, and  $n$  is the reaction order.  $k_f$  and  $n$  were determined by plotting  $\log(v_a)$  vs.  $(\log[A_0])$ . Reaction rate data were also used to determine Michaelis–Menten parameters ( $k_{\text{cat}}$  and  $K_m$ ) as described in supplemental information (see Appendix A).

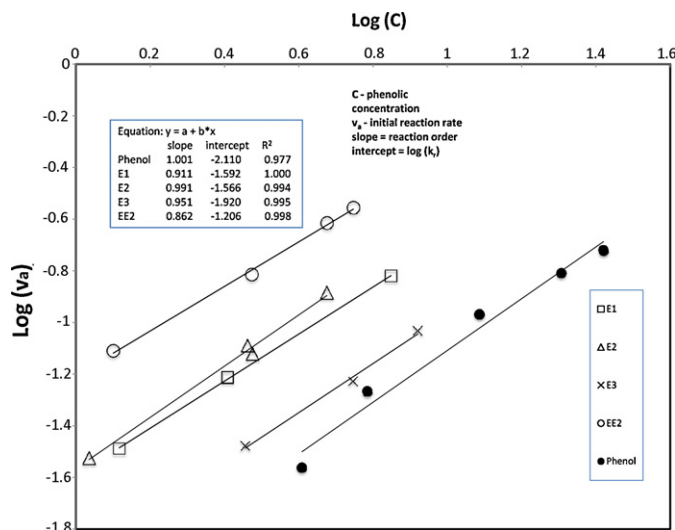


Fig. 1. Initial reaction rates. E<sub>1</sub>, E<sub>2</sub>, E<sub>3</sub>, EE<sub>2</sub>, and phenol.

The reaction rate constant was determined at different temperatures using the following [12]:

$$\frac{v_{aT}}{v_{a298K}} = \frac{(k_f[B_0]^m)[A_0]^n}{(k_{f298K}[B_0]^m)[A_0]^n} = \frac{k_{fT}}{k_{f298K}} \quad (2)$$

Thermodynamic parameters  $\Delta H^*$  and  $\Delta S^*$  were determined using a linear regression of Eyring's equation:

$$\ln \frac{k}{T} = \frac{-\Delta H^*}{R} \times \frac{1}{T} + \ln \frac{k_B}{h} + \frac{\Delta S^*}{R} \quad (3)$$

The Eyring equation was transformed by substituting  $k_r = k[B_0]^m$ ,  $[H_2O_2] = 10 \mu\text{M}$ , and  $m = 1$  [16]:

$$\ln \frac{k_f}{T} = \frac{-\Delta H^*}{R} \times \frac{1}{T} + \ln \frac{k_B}{h} + \frac{\Delta S^*}{R} - 9.21 \quad (4)$$

$R$  is the ideal gas constant (8.314 J/mol K),  $k_B$  is Boltzmann constant,  $h$  is Planck's constant, and  $T$  is temperature in Kelvin.

### 2.7. $E_{\text{HOMO}}$ calculation

The  $E_{\text{HOMO}}$  was determined using the Gaussian 03 program via the Pittsburgh supercomputer center. Structure optimization of the model compound was conducted with 6-31G (d) basis set at level of Unrestricted Hartree–Fock (UHF). After structure optimization,  $E_{\text{HOMO}}$  of the model compounds were calculated in the same method and basis set.

### 2.8. Docking simulations

Autodock 4.2 was used to simulate the binding between the five phenolic compounds and HRP. At least ten confirmations were possible for each substrate, and for the purposes of this comparative study, the confirmation that was selected had the lowest binding energy because lower energy states are more stable. The Lamarckian genetic algorithm (GA) method was used to calculate free energy changes. In Autodock 4.2, a docking box of  $100 \times 100 \times 100$  points was defined with a grid spacing of 0.375 Å. The structural coordinates of the model horseradish peroxidase compound II (1H55) were downloaded from the Research Collaboratory for Structural Bioinformatics Protein Data Bank (RCSBPDB). Then, the crystallographic water molecules were removed from the active site before docking, and the hydrogen atoms and partial charges were added using the Amber force field. Partial charges were assigned to HRP and the phenolic substrates using the Gasteiger Partial Equalization of Orbital Electronegativities method. The coordinates of phenolic substrate were used as the initial position for the docking simulation, and HRP was superimposed onto the phenolic substrate to obtain an initial position. The flexible amino acids residues were HIS42, ARG38, PHE41, and ASN70. The binding distance was between the substrate's phenolic proton and the imidazole  $\delta\text{N}$  on the HIS42 residue as suggested previously [1].

## 3. Results and discussion

### 3.1. Kinetics

Fig. 1 shows the two-dimensional logarithmic graphs associated with the oxidative coupling reactions carried out in this study. The

**Table 1**  
Michaelis–Menten parameters and second order reaction rate constants ( $T = 25^\circ\text{C}$ ).

Compound	Michaelis–Menten model					
	$K_m$ ( $\mu\text{M}$ ) <sup>a</sup>	$k_{\text{cat}}$ ( $\text{s}^{-1}$ ) <sup>b</sup>	Apparent second order rate constant $k$ ( $k_{\text{cat}}/K_m$ ) ( $\text{M}^{-1} \text{s}^{-1}$ )	Collision theory rate constant ( $k^{\text{coll}}$ ) ( $\text{M}^{-1} \text{s}^{-1}$ )	Radii ( $r_b$ ) ( $\text{\AA}$ )	Diffusion coefficient ( $D_B$ ) ( $\text{cm}^2/\text{s}$ ) <sup>c</sup>
Phenol	94	0.83	$8.85 \times 10^3$	$1.89 \times 10^{10}$	3.3	$7.43\text{E}-6$
E <sub>1</sub>	24	0.57	$2.42 \times 10^4$	$1.48 \times 10^{10}$	4.5	$5.45\text{E}-6$
E <sub>2</sub>	78	1.42	$1.81 \times 10^4$	$1.48 \times 10^{10}$	4.5	$5.45\text{E}-6$
E <sub>3</sub>	60	0.67	$1.13 \times 10^4$	$1.48 \times 10^{10}$	4.5	$5.45\text{E}-6$
EE <sub>2</sub>	15	0.86	$5.89 \times 10^4$	$1.45 \times 10^{10}$	4.6	$5.33\text{E}-6$

<sup>a</sup> The absolute values of  $K_m$  are to be regarded as estimates because the phenolic concentrations used in this research were generally smaller than these  $K_m$  values. However, the accuracy of this data is sufficient to help distinguish between kinetically limited and collision rate-limited reaction rates because of the large differences in the rate constants.

<sup>b</sup>  $k_{\text{cat}} = v_{\text{max}}/[E_t]$ , where  $[E_t]$  is the HPR concentration.

<sup>c</sup> Calculated with the Stokes–Einstein equation as described in Appendix B.

initial reaction rate was highest for EE<sub>2</sub>, followed by (in order) E<sub>2</sub>, E<sub>1</sub>, E<sub>3</sub> and phenol. The slopes of the log–log regressions reveal the reaction order, which was close to 1 for all the substrates. This is in keeping with the findings of Auriol et al. [3]. The y-intercept of each regression is the log ( $k_r$ ). This value is greatest for EE<sub>2</sub> (−1.206), followed by E<sub>2</sub> (−1.566), E<sub>1</sub> (−1.592), E<sub>3</sub> (−1.920), and phenol (−2.110). These kinetic differences are strongly influenced by substrate affinity, and this is shown in three ways. First, the previously published Michaelis–Menten half saturation parameters ( $K_m$ ) indicate the relative affinity for each substrate toward HRP. Relatively small values of  $K_m$  reflect high affinity, and previously published data [4] show that HRP has the greatest affinity for EE<sub>2</sub> ( $K_m = 15 \mu\text{M}$ ) followed by (in decreasing order), E<sub>1</sub> (24  $\mu\text{M}$ ), E<sub>3</sub> (60  $\mu\text{M}$ ), E<sub>2</sub> (78  $\mu\text{M}$ ), and phenol (94  $\mu\text{M}$ ). This  $K_m$  order is generally consistent with the aforementioned reaction rate order (although the  $K_m$  for E<sub>2</sub> is an exception). Second, the observed reaction rate constants were compared to the collision rate-limited maximum reaction rate constant (see Appendix B for details), and the results show that the second order bimolecular collision rate constant ( $k^{\text{coll}}$ ) was on the order of  $10^{10} \text{M}^{-1} \text{s}^{-1}$ , which is several orders of magnitude higher than our observed rate constants or those reported by Auriol et al. [3] (i.e.  $1.56 \times 10^6 \text{M}^{-1} \text{s}^{-1}$ ) (Table 1). Third,  $k_r$  does not correlate with  $k_{\text{cat}}$  (see Appendix C). For example, phenol and EE<sub>2</sub> have similar  $k_{\text{cat}}$  values ( $k_{\text{cat}} = 0.83/\text{s}$  for phenol and  $k_{\text{cat}} = 0.86/\text{s}$  for EE<sub>2</sub>) but very different observed reaction rate constants. Similarly, E<sub>1</sub> reacts faster than E<sub>3</sub>, but its  $k_{\text{cat}}$  value (0.57/s for E<sub>1</sub> and 0.67/s for E<sub>3</sub>) is lower than that of E<sub>3</sub>. Similar observations can be made with data published previously by Auriol et al. [3]. Interestingly,  $k_{\text{cat}}$  is positively correlated with  $E_{\text{HOMO}}$  [1], which makes sense because  $k_{\text{cat}}$  and  $E_{\text{HOMO}}$  relate to the maximum reaction rate potential. The results also show that  $k_r$  does not correlate well with  $E_{\text{HOMO}}$  (see Appendix D). OXC kinetics do not depend solely on reaction rate potential and they are not collision rate-limited, but instead they are controlled by enzyme–substrate interactions.

### 3.2. Molecular volume and substrate binding

This study determined the molecular volume of the substrates and two aspects of substrate binding, binding distance and energy. Molecular volume (MV) affects the accessibility of the compound to the active site pocket of the HRP. The steroidal hormones have a similar molecular volume (between 230 and 244  $\text{cm}^3/\text{mol}$ ), but phenol has a lower value (87.8  $\text{cm}^3/\text{mol}$ ). Phenol also has the smallest reaction rate constant. EE<sub>2</sub> occupies the largest molecular volume ( $MV = 244.4 \text{cm}^3/\text{mol}$ ) and reacts with the highest rate. This shows that molecular volume does not limit substrate reactivity. In principle, a larger compound may react slower due to steric hindrance, but this was not observed in the current study. Fig. 2

shows the binding energy values, which are in principle determined by the complementarity of enzyme and substrate. The strength of these bonds depends on minimizing steric repulsion, the presence of unsolvated or unpaired charges, and sufficient hydrogen bonding. Binding energy reduces the free energy of the transition state, allowing for more favorable interactions. Phenol has the least favorable binding energy (−3.54 kcal/mol), releasing the smallest amount of free energy when it forms weak interactions with HRP. The other 4 compounds have higher binding energy values (i.e. E<sub>2</sub> (−6.45 kcal/mol), EE<sub>2</sub> (−7.14 kcal/mol), E<sub>1</sub> (−7.6 kcal/mol) and E<sub>3</sub> (−5.8 kcal/mol)). These binding energy values are largely in line with binding distance values. Our simulations showed that phenol had the longest binding distance (7.05  $\text{\AA}$ ), as expected, while the binding distances for the four hormones were 6.09  $\text{\AA}$  (E<sub>1</sub>), 6.04  $\text{\AA}$  (E<sub>3</sub>), 5.83  $\text{\AA}$  (E<sub>2</sub>), and 6.47  $\text{\AA}$  (EE<sub>2</sub>). The longer binding distance helps explain why phenol is removed more slowly than the four hormones, which appear to fit the active site better than phenol does, even though their molecular volume is larger than that of phenol.

### 3.3. Thermodynamic parameters

Fig. 3 shows that at each temperature, EE<sub>2</sub> had the largest reaction rate constant, followed by E<sub>2</sub>, E<sub>1</sub>, E<sub>3</sub> and phenol. The slopes of the linear regressions are negative, meaning that higher temperatures correspond to higher reaction rate constants. Meanwhile, the slopes are inversely related to the enthalpy of activation, which represents the difference in energy between the transition state and the ground state. As all the slopes are negative, the results

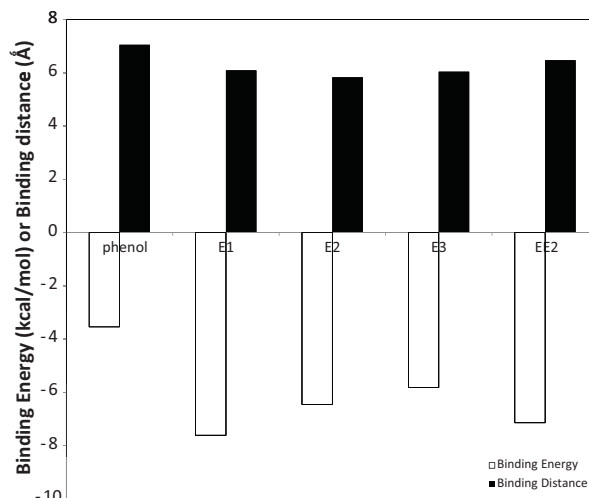


**Fig. 2.** Substrate binding: binding energy and binding distance.

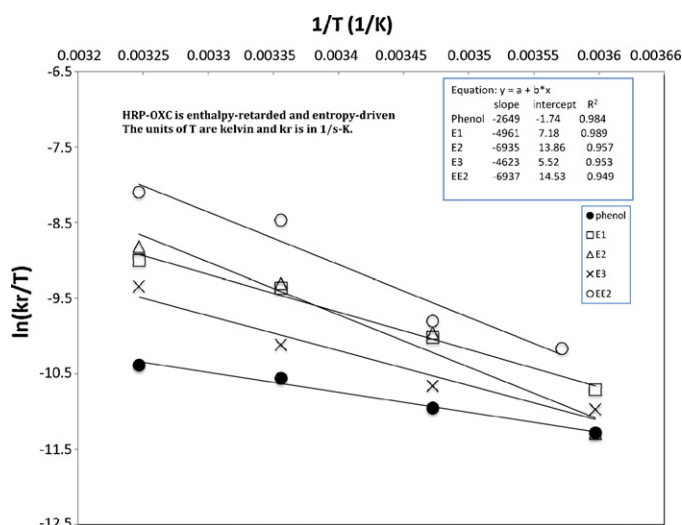


Fig. 3.  $\ln(k_r/T)$  vs.  $1/T$ . Phenol, E<sub>1</sub>, E<sub>2</sub>, E<sub>3</sub>, and EE<sub>2</sub>.

show that the activation enthalpies are positive and have values that decrease in the following order: EE<sub>2</sub> (57.7 kJ K<sup>-1</sup> mol<sup>-1</sup>), E<sub>2</sub> (57.7 kJ K<sup>-1</sup> mol<sup>-1</sup>), E<sub>1</sub> (41.2 kJ K<sup>-1</sup> mol<sup>-1</sup>), E<sub>3</sub> (38.4 kJ K<sup>-1</sup> mol<sup>-1</sup>) and phenol (22.0 kJ K<sup>-1</sup> mol<sup>-1</sup>). The activation entropies are related to the y-intercept and they decrease in the following order: EE<sub>2</sub> (18.9 J/mol), E<sub>2</sub> (13.4 J/mol), E<sub>1</sub> (-42.1 J/mol), E<sub>3</sub> (-55.9 J/mol) and phenol (-116.3 J/mol). The reaction rates increase with activation entropies and they decrease as the activation enthalpies increase. This means that HRP-OXC is entropy-driven and enthalpy retarded.

A higher (i.e. more positive) activation entropy value implies a more flexible binding structure in the active site pocket. Before substrate binding, phenolics are coated with water molecules (i.e. they have a solvation shell) so as to maximize hydrogen bonding and decrease entropy [17]. The active site also hosts a rigid and ordered structure because of the interaction of the residues, the heme, and the solute matrix in the substrate access channel [18]. Thus, the solution system starts at low entropy. When the substrate enters the active pocket, the solvation shell (i.e. water molecules) is at least partially lost because some of these water molecules do not fit into the active site and because new active site interactions are formed [e.g. 19–21]. These dynamics help shed light on the observations made in this study. For example, the phenol had a lower reaction rate constant and a larger binding distance, compared to the four hormones. This leads to the hypothesis that these higher reaction rates are possible when chemicals move deeper into the active site pocket, which can destroy the solvation shell to a higher extent and may lead to the higher entropy change if new chemical bonds permit many degrees of freedom. It is possible that some hormones may move deep into the active site but not trigger the high entropy change because new chemical bonds may create rigidity. Isothermal titration calorimetry can be done in future experiments to address these ideas.

The thermodynamic data can be used to raise two additional ideas. First, the results show a strong linear relationship ( $R^2 = 0.99$ ) between enthalpy and entropy (Fig. 4). Changes in enthalpy are seen to be compensated for with associated changes in entropy, so this now refers to enthalpy–entropy compensation theory. This idea is somewhat controversial, because linearity in enthalpy–entropy relationships may be caused by statistical artifacts [22]. However, for aqueous reactions involving enzymes and small molecules, there is measured data that not only supports compensation theory, but that also shows that water molecules affect enzymatic activity [23–25]. For example, Kocherbitov and Arnebrant [25] used measured calorimetric data to show that

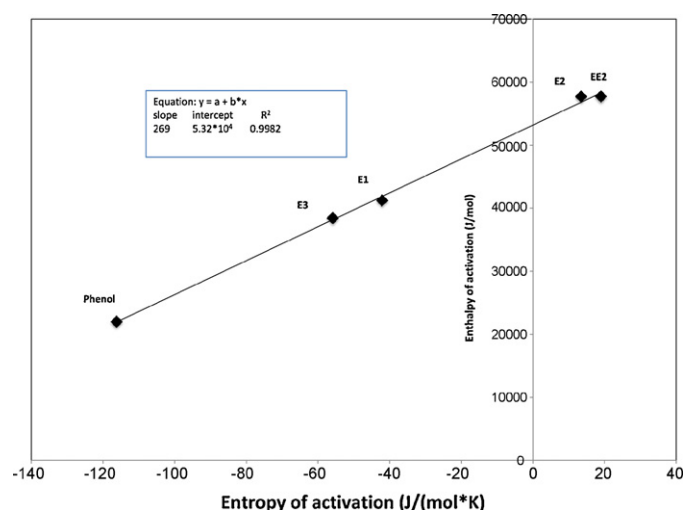


Fig. 4. Activation enthalpy and entropy.

enthalpy–entropy compensation is relevant to the activity of lysozyme and that the adsorption of water molecules impacted the confirmation of the protein. Reynolds and Holloway analyzed measured thermodynamic data for 100 protein–ligand interactions and they found that enthalpy–entropy compensation theory was clearly supported over a broad range of enzymes and substrates [26]. Enthalpy–entropy relationships are related to real phenomenon. The data in this current study support the idea that water molecules play in HRP-OXC and future experiments should attempt to address this definitively by directly measuring both enthalpy and entropy. Second, the values of the activation entropies are, in principle, related to reaction mechanisms [27–29]. Activation entropy includes two contributions, one related to a change in the rotational and translational freedom of the reacting species and a second related to interactions with the solvent. The results show that the slowest reacting chemicals (e.g. phenol) had negative activation entropy and that the fastest reacting hormone (e.g. EE<sub>2</sub>) had positive activation entropy. This suggests that subtle electron exchange distinctions may be associated with significant kinetic implications, but this issue can not be further clarified at this time because it is not clear what parts of these entropies are intrinsic to the electron exchange reaction and what parts are associated with solvation entropies. Fortunately, this issue can be addressed in future research with computational approaches that provide a careful accounting for all chemical interactions that influence entropy [30].

#### 4. Conclusions

In this study, various factors affecting substrate reactivity were evaluated during HRP-OXC of phenolic chemicals. Reactions were first order with respect to phenolic concentration and reaction rate constants ( $k_r$ ) were determined for phenol, E<sub>3</sub>, E<sub>1</sub>, E<sub>2</sub> and EE<sub>2</sub> (in increasing order). Structurally similar chemicals can be oxidatively polymerized at very different rates. These reactions were not collision rate-limited, but instead were controlled by enzyme–substrate interactions. Binding energy and distance both explain why phenol is removed more slowly than the four hormones, but other contributing factors appear to influence reaction rates. The molecular volume of the substrates did not impact reaction rates, likely because the HRP active site is large enough to accommodate all of the phenolic chemicals that were removed. Further, the thermodynamic parameters showed positive activation enthalpies and negative activation entropies. HRP-OXC is entropy-driven and enthalpy retarded. Future experiments should further

investigate the values of the entropy changes that occur upon formation of the transition state.

### Acknowledgments

Funding for this work was provided by the National Science Foundation (NSF Grant No. 0506388). Any opinions, findings and conclusions or recommendations expressed in this material are those of the authors and do not necessarily reflect the views of NSF. The authors thank William Barr (PhD student, University of Pittsburgh) for assistance with the substrate structure optimization and  $E_{\text{HOMO}}$  calculation. The authors also thank the anonymous reviewers for their suggestions.

### Appendix A. Supplementary data

Supplementary data associated with this article can be found, in the online version, at doi:10.1016/j.enzmictec.2011.12.005.

### References

- Colosi ML, Huang Q, Weber WJ. Quantitative structure–activity relationship based quantification of the impacts of enzyme–substrate binding on rates of peroxidase-mediated reactions of estrogenic phenolic chemicals. *J Am Chem Soc* 2006;128:4041–7.
- Auriol M, Filali-Meknassi Y, Adams CD, Tyagi RD. Natural and synthetic hormone removal using the horseradish peroxidase enzyme: temperature and pH effects. *Water Res* 2006;40:2847–56.
- Auriol M, Filali-Meknassi Y, Tyagi RD, Adams CD. Oxidation of natural and synthetic hormones by the horseradish peroxidase enzyme in wastewater. *Chemosphere* 2007;68:1830–7.
- Zheng W, Colosi LM. Peroxidase-mediated removal of endocrine disrupting compound mixtures from water. *Chemosphere* 2011;85:553–7.
- Job D, Dunford HB. Substituent effect on the oxidation of phenols and aromatic amines by horseradish peroxidase compound I. *Eur J Biochem* 1976;66:607–14.
- Sakurada J, Sekiguchi R, Sato K, Hosoya T. Kinetic and molecular orbital studies on the rate of oxidation of monosubstituted phenols and anilines by horseradish peroxidase compound II. *Biochemistry* 1990;29:4093–8.
- Brewster ME, Doerge DR, Huang MJ, Kaminski JJ, Pop E, Bodor N. Application of semi-empirical molecular orbital techniques to the study of peroxidase-mediated oxidation of phenols, anilines, sulfides and thiobenzamide. *Tetrahedron* 1991;47:7525–36.
- Hosoya T, Fujii T, Ogawa S. A molecular orbital study on the oxidation of hydrogen donor molecules by peroxidase compound II. *J Theor Biol* 1983;100:283–92.
- Colosi LM, Huang Q, Weber WJ. QSAR-assisted design of an environmental catalyst for enhanced estrogen remediation. *Chemosphere* 2010;81:897–903.
- Janssen AEM, Sijnsnes BJ, Vakurov AV, Hall PJ. Kinetics of lipase-catalyzed esterification in organic media: correct model and solvent effects on parameters. *Enzyme Microb Technol* 1999;24:463–70.
- Wagner M, Nicell JA. Detoxification of phenolic solutions with horseradish peroxidase and hydrogen peroxide. *Water Res* 2002;36:4041–52.
- Blanch HW, Clark DS. *Biochemical engineering*. Marcel Dekker Publishers; 1997, 702 pp.
- Nakamoto S, Machida N. Phenol removal from aqueous solutions by peroxidase-catalyzed reaction using additives. *Water Res* 1992;26:49–54.
- Sakurai A, Toyoda S, Sakakibara M. Removal of bisphenol A by polymerization and precipitation method using *Coprinuscinerus peroxidase*. *Biotechnol Lett* 2001;23:995–8.
- Kinsley C, Nicell JA. Treatment of aqueous phenol with soybean peroxidase in the presence of polyethylene glycol. *Bioresour Technol* 2000;73:139–46.
- Yu J, Taylor KE, Zou HX, Biswas N, Bewtra JK. Phenol conversion and dimetic intermediates in the horseradish peroxidase-catalyzed phenol removal from water. *Environ Sci Technol* 1994;28:2154–60.
- Frank HS, Evans MW. Free volume and entropy in condensed systems. III. Entropy in binary liquid mixtures; partial molal entropy in dilute solution; structure and thermodynamics in aqueous electrolytes. *J Chem Phys* 1945;13:507–32.
- Vlasits J, Bellei M, Jakopitsch C, Rienzo FD, Furtmüller PG, Zamocky M, et al. Disruption of the H-bond network in the main access channel of catalase-peroxidase modulates enthalpy and entropy of Fe(III) reduction. *J Inorg Biochem* 2010;104:648–56.
- Israelachvili J, Wennerstrom H. Role of hydration and water structure in biological and colloidal interactions. *Nature* 1996;379:219–25.
- Barillari C, Taylor J, Viner R, Essex JW. Classification of water molecules in protein binding sites. *J Am Chem Soc* 2007;129:2577–87.
- Homans SW. Water, water everywhere—except where it matters. *Drug Discov Today* 2007;12:534–9.
- Cornish-Bowden A. Enthalpy–entropy compensation: a phantom phenomenon. *J Biosci* 2002;27:126–7.
- Lumry R, Rajender S. Enthalpy–entropy compensation phenomena in water solutions of proteins and small molecules: a ubiquitous property of water. *Biopolymers* 1970;9:1125–227.
- Kinoshita M. Roles of translational motion of water molecules in sustaining life. *Front Biosci* 2009;14:3419–48.
- Kocherbitov V, Arnebrant T. Hydration of lysozyme: the protein–protein interface and the enthalpy–entropy compensation. *Langmuir* 2010;26:3918–22.
- Reynolds C, Holloway K. Thermodynamics of ligand binding and efficiency. *ACS Med Chem Lett* 2011;2:433–7.
- Stearn A, Johnston H, Clark C. The significance of activation entropy in catalytic mechanisms. *J Chem Phys* 1939;7:970–1.
- Villa J, Strajbl M, Glennon T, Sham Y, Chu Z, Warshel A. How important are entropic contributions to enzyme catalysis. *Proc Natl Acad Sci* 2000;97:11899–904.
- Milischuk A, Matyushov D, Newton M. Activation entropy in electron transfer reactions. *Chem Phys* 2006;324:172–94.
- Kamerlin S, Florian J, Warshel A. Associative versus dissociative mechanisms of phosphate monoester hydrolysis: on the interpretation of activation entropies. *ChemPhysChem* 2008;9:1767–73.